View Article Online
View Journal

Dalton Transactions

An international journal of inorganic chemistry

Accepted Manuscript

This article can be cited before page numbers have been issued, to do this please use: T. Zhang and L. Ye, *Dalton Trans.*, 2026, DOI: 10.1039/D6DT00435K.

This is an Accepted Manuscript, which has been through the Royal Society of Chemistry peer review process and has been accepted for publication.

Accepted Manuscripts are published online shortly after acceptance, before technical editing, formatting and proof reading. Using this free service, authors can make their results available to the community, in citable form, before we publish the edited article. We will replace this Accepted Manuscript with the edited and formatted Advance Article as soon as it is available.

You can find more information about Accepted Manuscripts in the Information for Authors.

Please note that technical editing may introduce minor changes to the text and/or graphics, which may alter content. The journal's standard Terms & Conditions and the Ethical guidelines still apply. In no event shall the Royal Society of Chemistry be held responsible for any errors or omissions in this Accepted Manuscript or any consequences arising from the use of any information it contains.

ROYAL SOCIETY OF CHEMISTRY

rsc.li/dalton

ARTICLE Journal Name

Minimalist Second-Sphere Engineering with Polyvinyl Alcohol Drives Cooperative Hydrolysis in Zn(II) System

View Article Online
DOI: 10.1039/D6DT00435K

Tong Zhang [a] and Lei Ye *[a]

Received 00th January 20xx,
Accepted 00th January 20xx

DOI: 10.1039/x0xx00000x

First sphere engineering has enabled potent artificial phosphatases, but strategies that generate enzyme-like second-sphere effects with simple disordered materials remain limited. Here we demonstrate that partially hydrolyzed polyvinyl alcohol (PVA80, 80% hydrolyzed) acts as a minimalist soft matter scaffold that amplifies the hydrolytic activity of hydrated Zn(II). Rather than functioning as a static host, the amphiphilic polymer undergoes substrate induced reorganization to form hydrophobic microdomains. These microdomains enrich the substrate and organize labile Zn(II) into cooperative catalytic networks that exhibit cooperative kinetics with a Hill coefficient of 4.2, and selectivity for hydrophobic substrates. The catalyst has an apparent Michaelis-Menten constant (K_M) of 0.52 mM and a catalytic efficiency (k_{cat}/K_M) of 1.86×10^{-2} M^{-1} s^{-1}, approaching the performance of synthetic Zn(II) phosphoesterases based on Zn(II) complexes. Solvatochromic and solvent isotope analyses indicate that rate enhancement arises from coupled hydrophobic partitioning and polymer assisted proton transfer. In contrast, Ce(IV) retains Michaelis-Menten behavior upon polymer addition, with PVA80 primarily enhancing substrate availability without inducing cooperative activation. These findings show that enzyme like behavior can emerge from disordered polymer interfaces, and simple polymer chains can provide an accessible strategy to modulate metal reactivity without complicated synthesis.

Metal catalyzed hydrolysis of phosphate esters remains a longstanding challenge in biomimetic chemistry due to the intrinsic inertness and kinetic stability of the phosphoester bond.[1] Most artificial phosphatases have been developed by tuning the primary coordination sphere of metal ions through multidentate ligands,[2, 3] metallosupramolecular assemblies,[4] metal organic frameworks[5, 6] and structurally defined nanozymes.[7, 8] While these constructs enhance reactivity by stabilizing specific metal ligand geometries or enabling multinuclear configurations, they typically rely on static architectures that require elaborate synthesis and strict structural preorganization. Consequently, their catalytic behavior is frequently dominated by first sphere electronic factors while the broader adaptive microenvironmental influences analogous to those in enzymatic catalysis remain less explored.

In natural metalloenzymes, substantial rate enhancements arise not only from the arrangement of metal-coordinating residues but also from second-sphere interactions including hydrophobic pockets, hydrogen-bonding networks, conformational dynamics and proton-transfer motifs.[9, 10] These features create responsive environments that regulate substrate positioning and stabilize transition states.[11] While artificial enzyme designs incorporating second-sphere interactions have begun to emerge,[10, 12] synthetically simple strategies for imparting enzyme-like second-sphere functionality to hydrated metal ions remain limited.

In many natural phosphatases Zn(II) ions serve as catalytic metal centers, where binuclear Zn(II) sites promote hydrolysis of phosphate ester through direct substrate coordination and transition state stabilization.[13, 14] Inspired by these systems, Zn(II) has been widely explored in artificial phosphatase models.[15-17] In aqueous solution free Zn(II) exhibits a highly labile d^{10} coordination environment that forms equilibria between aquo and hydroxo species and rarely produces persistent multinuclear structures that activate phosphate esters.[18-20] As a result the free Zn(II) system shows weak hydrolytic activity. Polyvinyl alcohol (PVA) is a simple and biocompatible polymer whose amphiphilicity can be readily tuned through partial hydrolysis, resulting in materials that combine hydrophilic hydroxyl groups with residual acetate functionalities and have found broad use in aqueous applications.[21, 22]

Here we demonstrate that partially hydrolyzed PVA can serve as a minimalist soft matter scaffold capable of exerting macromolecular second-sphere control on metal mediated phosphate hydrolysis (Figure 1). Rather than acting as a static host, the amphiphilic polymer undergoes a substrate induced reorganization to generate dense hydrophobic microdomains. These compartments efficiently enrich the substrate and organize labile Zn(II) ions into cooperative catalytic networks that exhibit pronounced cooperative kinetics and selectivity for hydrophobic substrates. In contrast, Ce(IV) species, which already exhibit efficient substrate binding and Michaelis–Menten kinetics, respond to PVA80 primarily through enhanced substrate enrichment but do not display cooperative activation. These findings establish that sophisticated enzyme-like behavior can emerge from disordered polymer interfaces, and offer an accessible strategy to modulate metal reactivity without relying on structural precision.

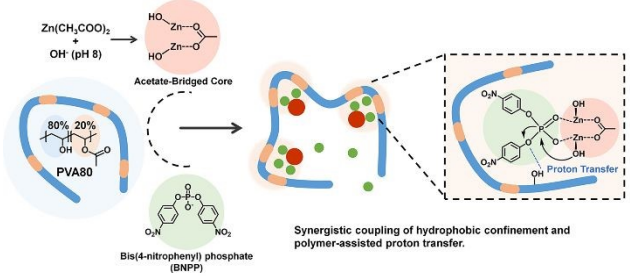

Figure 1. Schematic illustration of minimalist second-sphere control enabled by polyvinyl alcohol.

PVA samples with different degrees of hydrolysis (DH) were prepared and characterized by comparing the acetate band intensities in the FTIR spectra (Figure S1).[23] To evaluate the influence of DH, the polymers were introduced into the Zn(II) catalyzed hydrolysis of bis(4-nitrophenyl) phosphate (BNPP). As shown in

[a] Division of Pure and Applied Biochemistry, Department of Chemistry, Lund University, Lund 22100, Sweden. Email: lei.ye@tbiokem.lth.se
Supplementary Information available: [details of any supplementary information available should be included here]. See DOI: 10.1039/x0xx00000x

View Article Online
DOI: 10.1039/D6DT00435K

Figure 2a, PVA80 (80% hydrolyzed) markedly accelerated the reaction and increased the initial rate by 16.3-fold relative to free Zn(II). PVA90 produced a minor enhancement, while fully hydrolyzed PVA100, ethylene glycol (EG) and polyethylene glycol (PEG) showed no measurable effect. Control experiments showed that PVA80 alone does not hydrolyze BNPP. In addition, to exclude potential optical artifacts arising from light scattering by aggregates, the system was continuously monitored at pH 8.0 at the detection wavelength of the *p*-nitrophenolate product in the absence of substrate. Despite the formation of aggregates, the absorbance baseline remained stable and unchanged (Figure S2), confirming that the observed signal increase in catalytic experiments originates from product formation rather than scattering effects. The different behavior of the three PVA polymers indicates that a specific balance of hydrophobic and hydrophilic segments is critical for promoting catalysis. Dynamic light scattering (DLS) measurements (Figure S3) show that Zn(II) system forms flocculent aggregates under the reaction conditions both in the absence and presence of PVA80. As shown in Figure 2b, removal of the insoluble aggregates by centrifugation at the 5 min time point led to an almost complete loss of activity in the supernatant. This result establishes that the activity is confined to the aggregated phase and that the soluble zinc species do not contribute to catalysis. To examine the coordination environment of the zinc within these aggregates we analyzed the solid species isolated from the Zn(II)-PVA80 system by FTIR (Figure 2c). Both the Zn(II) and Zn(II)-PVA80 samples display acetate signals, indicating the formation of acetate-bridged multinuclear Zn-OH clusters, which act as the active catalytic core. Zinc acetate was selected because acetate acts as a stable bridging ligand and promotes the formation of multinuclear Zn(II) species that show higher catalytic activity toward BNPP hydrolysis than zinc nitrate or zinc chloride (Figure S4). The spectrum lacks the characteristic bands at 1735 cm^{-1} (C=O) or 1240 cm^{-1} (C-O-C) which are associated with the PVA80. The absence of these signals shows that the aggregates do not contain detectable PVA80 and that PVA80 does not form a stable inner sphere complex with Zn(II).

To further probe the interaction between Zn(II) species and PVA80, X-ray photoelectron spectroscopy (XPS) was used to examine the isolated solids. Compared with the Zn(II) sample, the Zn(II)-PVA80 material shows a higher oxygen atomic percentage and a lower zinc content (Table S1), consistent with retention of a small amount of PVA80 within the dried aggregates, below the detection limit of FTIR. The Zn 2p spectra are identical in binding energy and line shape for both samples (Figure S5), indicating that incorporation of PVA80 does not alter the electronic state of Zn(II). This result supports the absence of strong inner sphere coordination. In the O 1s region, the Zn(II) sample exhibits a low-binding-energy shoulder that reflects heterogeneous oxygen environments associated with Zn-O(H) species. Upon addition of PVA80, this feature is no longer resolved and the O 1s envelope becomes smoother and more symmetric, suggesting partial homogenization of surface oxygen environments. Such homogenization of the Zn-O coordination environment may contribute to the enhanced catalytic activity observed for BNPP hydrolysis.[24]

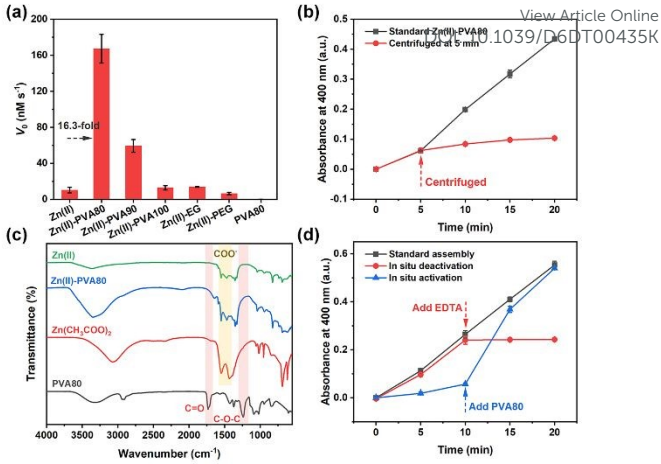

Figure 2. (a) Initial hydrolysis rates (V_0) of BNPP catalyzed by Zn(II) in the presence of PVA derivatives with varying DH compared with ethylene glycol (EG) and polyethylene glycol (PEG) controls. (b) Hot-centrifugation analysis monitoring the reaction kinetics of the supernatant isolated after removing catalytically active aggregated phase at 5 min (red trace) compared to the ongoing heterogeneous suspension (black trace). (c) FTIR spectra of pure PVA80, zinc acetate, and the solid precipitate isolated from the Zn(II) or Zn(II)-PVA80 mixture. (d) Dynamic response of the catalytic system monitoring BNPP hydrolysis (absorbance at 400 nm) versus time. The traces illustrate the immediate activation upon adding PVA80 to a free Zn(II) solution and the rapid inhibition upon adding EDTA (2.0 mM) to an active Zn(II)-PVA80 system. Conditions: [Zn(II)] = 2.0 mM, [BNPP] = 2.0 mM, [additive] = 1.0 mg mL^{-1}, 50 mM HEPES buffer, pH 8.0, 37 °C.

The accessibility of the metal sites was examined through in situ inhibition and activation tests (Figure 2d). The immediate loss of activity after EDTA addition shows that the zinc centers remain accessible and that PVA80 does not block access. In contrast, rapid activation occurred when PVA80 was introduced into an initially low activity Zn(II) system. This response indicates rapid formation of a catalytically competent assembly and supports the view that PVA80 acts as an adaptive second-sphere scaffold that creates a microenvironment favorable for catalysis through noncovalent interactions with dynamic characteristics.

Hydrolysis rates were next evaluated as a function of Zn(II) and PVA80 concentrations. Figure S6 illustrates the activity profile at a fixed PVA80 concentration of 1.0 mg mL^{-1} with varying Zn(II) loading. While free Zn(II) requires concentrations above 1.0 mM to show detectable activity, the presence of PVA80 enables catalysis at lower levels. As the Zn(II) concentration exceeds 2.0 mM, the rate enhancement plateaus. Control experiments at high Zn(II) loading with increasing PVA80 showed a continuous rate increase, which indicates that the plateau arises from saturation of polymer binding sites rather than metal inhibition (Figure S7). At a fixed Zn(II) concentration of 2.0 mM the activity profile identifies the PVA80 saturation point of the hybrid system (Figure S8). Based on these analyses a composition containing 2.0 mM Zn(II) and 1.0 mg mL^{-1} PVA80 was selected for subsequent kinetic measurements. The pH dependence and stability of the active species were then examined. Product yields collected after 1.5 h of reaction were used to avoid interference from turbidity caused by zinc hydroxide precipitation at alkaline pH. Free Zn(II) operates only between pH 7.5

View Article Online
DOI: 10.1039/D6DT00437K

and 8.0 whereas the Zn(II)-PVA80 system remains active up to pH 9.5 (Figure S9). Both systems reach maximum efficiency at pH 8.0, but the polymer preserves activity at higher pH, offering an extended operational window where free Zn(II) precipitates and becomes inactive.

Under optimized conditions the free Zn(II) system at 45°C shows very low activity and a linear dependence on substrate concentration, consistent with weak binding (Figure 3a). The addition of PVA80 produces a sigmoidal rate profile. Fitting the kinetic data with Hill equation indicates substrate concentration dependent cooperativity in the Zn(II)-PVA80 system with a Hill coefficient of 4.2, an apparent Michaelis-Menten constant K_M of 0.52 mM and catalytic efficiency k_{cat}/K_M of 1.86×10^{-2} M^{-1} s^{-1}. These kinetic parameters are comparable to those of designed Zn(II) based artificial phosphoesterases (Table S2).[2, 3, 16, 25-28] Temperature dependent measurements at 25°C, 37°C and 45°C indicate that higher temperature accelerates the reaction and sharpens the sigmoidal transition (Figure S10), accompanied by a decrease in K_M from 0.84 mM to 0.52 mM. The increase in apparent substrate affinity at higher temperature suggests that the substrate binding is entropy-driven, consistent with a mechanism driven by hydrophobic interactions.[29] To probe the origin of the cooperativity, we analyzed kinetic parameters at varying PVA80 concentrations (Figure S11). At 0.1 mg mL^{-1}, weak cooperativity is observed (Hill coefficient = 1.5) with a high apparent K_M (~8.0 mM), reflecting a much lower substrate affinity compared to the optimized system. Increasing PVA80 concentration to 0.5 mg mL^{-1} raises the Hill coefficient to 3.0 and decreases K_M to 0.71 mM. This threshold polymer concentration suggests that a minimum polymer density is required to establish a microenvironment that enriches substrate near the catalytic Zn(II) species.

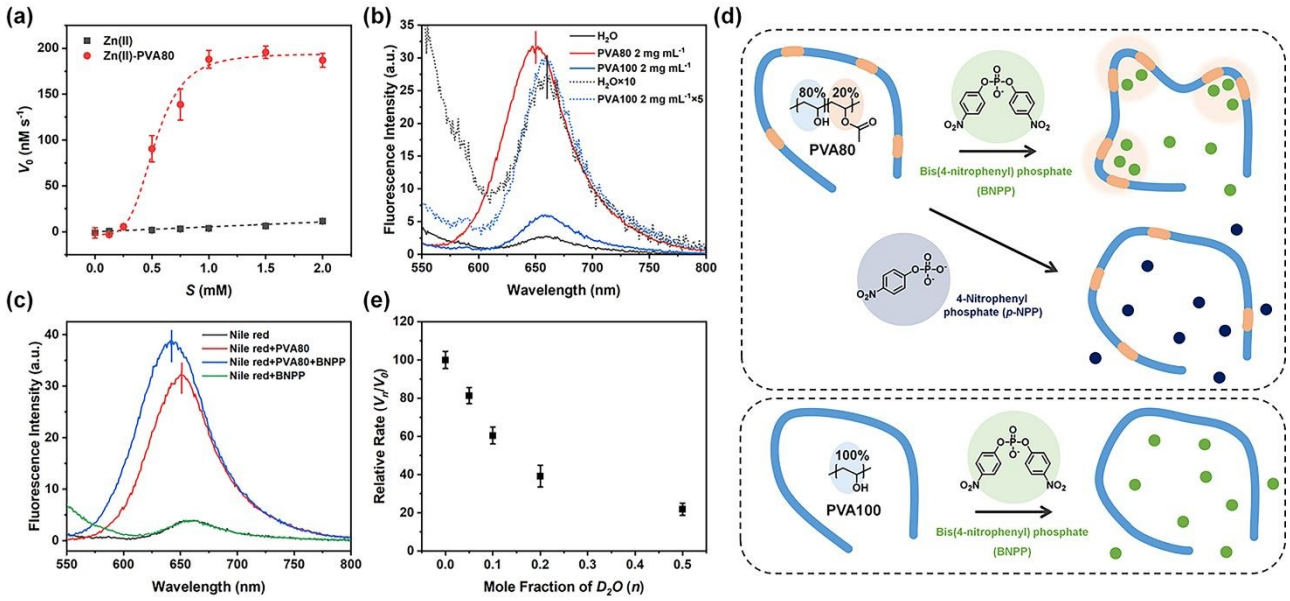

Figure 3. (a) Dependence of the initial hydrolysis rate on BNPP concentration. Free Zn(II) system (black) shows minimal activity within the tested range, whereas Zn(II)-PVA80 system (red) exhibits a sigmoidal profile that is fitted to the Hill equation with an apparent Hill coefficient of 4.2. (b) Fluorescence emission spectra of Nile Red (1 μM) with PVA80 or PVA100 (both at 1.0 mg mL^{-1}). (c) Effect of BNPP (2 mM) addition on the microenvironment polarity evidenced by Nile Red (1 μM) in PVA80 solution (1.0 mg mL^{-1}). (d) Schematic illustration of hydrophobic enrichment. (e) Solvent isotope dependence of the reaction rate plotted against the mole fraction of D_2O. Conditions: [Zn(II)] = 2.0 mM, [PVA80] = 1.0 mg mL^{-1}, [BNPP] = 2.0 mM, 50 mM HEPES buffer, pH 8.0, 45 °C (a) and 37 °C (e).

To evaluate hydrophobic microdomains, Nile Red was employed as a solvatochromic probe (Figure 3b). In pure water and in fully hydrolyzed PVA100, the dye shows minimal fluorescence characteristic of a highly polar environment. The introduction of amphiphilic PVA80 produces 11.5-fold fluorescence increase with a blue shifted emission maximum. These spectral changes indicate that PVA80 forms hydrophobic microdomains with localized low polarity regions that accommodate hydrophobic guests. Fully hydrolyzed PVA100 (which lacks the acetate side chains) shows no detectable enrichment of BNPP. The magnitude of the fluorescence enhancement and spectral shift correlates positively with PVA80 concentration (Figure S12). The addition of hydrophobic BNPP to the PVA80 system triggers further fluorescence enhancement and a more pronounced blue shift compared to PVA80 alone (Figure 3c), while BNPP itself produces no measurable spectral changes. The addition of hydrophilic substrate *p*-nitrophenyl phosphate (*p*-NPP) to the PVA80 system does not induce additional fluorescence enhancement or spectral shift (Figure S13). These observations suggest that BNPP occupies the hydrophobic regions of PVA80 and enhances their organization, allowing Nile Red to partition more strongly. *p*-NPP lacks the second aromatic ring and bears a dianionic phosphate group at neutral pH, which favors solvation and disfavors partitioning into low polarity domains. DLS measurements of PVA80 in the absence and presence of BNPP show nearly identical size distributions (Figure S14), indicating that these microdomains do not correspond to large-scale aggregates but rather reflect local polarity heterogeneity within the polymer network. Collectively, these observations support an enrichment model in which catalytic

amplification requires both a hydrophobic substrate and an amphiphilic polymer scaffold (Figure 3d).

The mechanism was further probed by solvent isotope effects using deuterium oxide (D_2O) (Figure 3e). The reaction rate in the Zn(II)-PVA80 system is strongly dependent on solvent composition and decreases nonlinearly as the D_2O fraction increases. At a mole fraction of 0.5 (50% D_2O) the rate falls to 21.8% of that in water, corresponding to an observed solvent isotope effect of 4.6 calculated from the 50% D_2O rate. The reaction becomes essentially inactive in pure D_2O (Figure S15). These observations are consistent with a rate limiting sequence involving proton transfers sensitive to isotopic substitution. The magnitude and profile of the solvent isotope effect are consistent with mechanisms involving multiple proton motions in the rate limiting transition state and with participation of a dense hydroxyl hydrogen bond network in proton transfer.[30, 31]

PVA80 was further examined in the Ce(IV) catalyzed system to assess whether its enhancement extends beyond Zn(II) under similar conditions. PVA samples with different DH exhibit distinct effects on the initial reaction rates of the Ce(IV) system (Figure 4a). PVA80 increases the rate by 2.2-fold. PVA90 produces only a minor enhancement and PVA100 shows no measurable improvement. Small molecular analogues such as ethylene glycol and polyethylene glycol do not promote the reaction. Kinetic analysis indicates that the Ce(IV) reactions conform to Michaelis-Menten behavior both without and with PVA80 (Figure 4b). The linear Lineweaver-Burk plots are consistent with this interpretation (Figure 4c and Table S2). In the presence of PVA80, the apparent K_M decreases from 1.75 mM to 0.92 mM while the k_{cat} increases modestly from 2.87×10^{-4} s^{-1} to 4.20×10^{-4} s^{-1}. These trends suggest that PVA80 primarily enhances substrate availability through hydrophobic partitioning, without leading to a pronounced change in the apparent turnover rate of Ce(IV). Ce(IV), as a strong Lewis acidic center that readily forms catalytically competent oxo/hydroxo oligomers in aqueous solution, already exhibits efficient phosphoester hydrolysis.[32-34] In contrast, aqueous Zn(II) species exhibit weak intrinsic substrate binding and linear kinetics, polymer mediated substrate enrichment, together with substrate promoted microdomain formation, induces a qualitative transition to cooperative behavior and accounts for the high catalytic efficiency observed in the Zn(II)-PVA80 system.

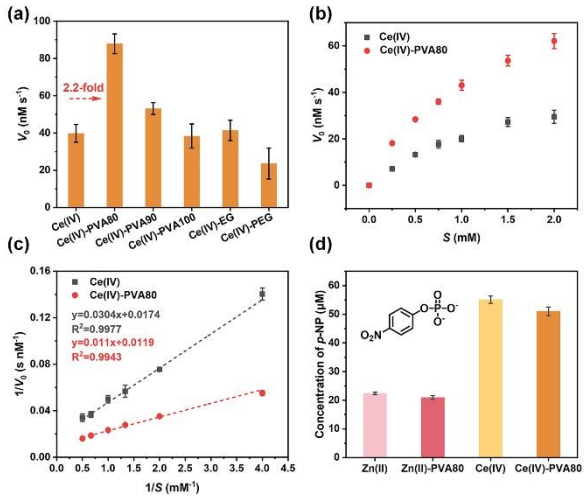

Figure 4. (a) Initial hydrolysis rates (V_0) of BNPP catalyzed by Ce(IV) in the presence of various PVA derivatives (with different DH), ethylene glycol (EG), and polyethylene glycol (PEG). (b) Michaelis-Menten kinetic profiles and (c) the corresponding Lineweaver-Burk double-reciprocal plots for the hydrolysis of BNPP catalyzed by Ce(IV). (d) Comparison of the concentration of *p*-nitrophenol (*p*-NP) produced after 1 h of reaction for the hydrophilic substrate *p*-nitrophenyl phosphate (*p*-NPP) catalyzed by Zn(II) and Ce(IV) in the absence and presence of PVA80. All reactions were conducted in 50 mM HEPES buffer at pH 8.0 and 37 °C. Conditions: (a) [Ce(IV)] = 0.2 mM, [BNPP] = 2.0 mM, [additive] = 1.0 mg mL^{-1}; (b, c) [Ce(IV)] = 0.2 mM, [PVA80] = 1.0 mg mL^{-1}; (d) [Zn(II)] = 2.0 mM, [Ce(IV)] = 0.2 mM, [*p*-NPP] = 4.0 mM, [PVA80] = 1.0 mg mL^{-1}.

Consistent with the proposed role of hydrophobic partitioning, the hydrophilic substrate *p*-NPP does not exhibit enhanced hydrolysis upon addition of PVA80 in either the Zn(II) or Ce(IV) systems (Figure 4d). The selectivity for hydrophobic substrate supports the conclusion that the polymer enhanced catalysis is restricted to substrates capable of effective partitioning within the PVA80 microenvironment under the conditions studied.

This study establishes that a minimalist amphiphilic polymer PVA80 can exert enzyme like second-sphere control on simple hydrated metal ions. Rather than functioning as a static host, PVA80 undergoes substrate-induced reorganization to generate dynamic low-polarity microdomains that selectively enrich hydrophobic substrates. Solvatochromic and solvent isotope measurements indicate that the rate enhancement arises from the coupling of hydrophobic partitioning and polymer assisted proton transfer. The contrasting responses of Zn(II) and Ce(IV) demonstrate that the emergence of cooperative kinetics depends on the interplay between polymer mediated microenvironments and the intrinsic substrate binding properties of the metal center. The simplicity of this PVA system highlights its potential as an accessible platform for tuning metal reactivity without requiring complicated molecular design. Future work will focus on systematically investigating the influence of polymer structural parameters to better understand and potentially tailor substrate selectivity, as well as extending this strategy to other metal systems and substrates. Collectively, these findings demonstrate that enzyme like activation can arise from disordered soft matter interfaces, and provide an accessible strategy for implementing second-sphere modulation in metal catalysis in aqueous environments.

Author contributions

Tong Zhang: Writing – original draft, Writing – review & editing, Investigation, Data curation, Formal analysis, Methodology, Conceptualization. Lei Ye: Writing – review & editing, Supervision, Project administration, Funding acquisition, Conceptualization.

Conflicts of interest

There are no conflicts to declare.

Data availability

The data supporting this article have been included as part of the SI. The supporting information contains experimental details on polymer preparation and characterization, spectroscopic analyses, catalytic assays.

Acknowledgements

This work was supported by the Carl Tryggers Foundation (CTS 23:2729), the Crafoord Foundation (20240526) and the Swedish Foundation for Strategic Research (SAB23-0003).

References

1 J. K. Lassila, J. G. Zalatan and D. Herschlag, *Annu. Rev. Biochem.*, 2011, **80**, 669–702.
2 N. Dutta, S. Haldar, G. Vijaykumar, S. Paul, A. P. Chattopadhyay, L. Carrella and M. Bera, *Inorg. Chem.*, 2018, **57**, 10802–10820.
3 J. Chen, X. Wang, Y. Zhu, J. Lin, X. Yang, Y. Li, Y. Lu and Z. Guo, *Inorg. Chem.*, 2005, **44**, 3422–3430.
4 Y. Wang, L. Yang, M. Wang, J. Zhang, W. Qi, R. Su and Z. He, *ACS Catal.*, 2021, **11**, 5839–5849.
5 K. Ma, Y. H. Cheung, K. O. Kirlikovali, H. Xie, K. B. Idrees, X. Wang, T. Islamoglu, J. H. Xin and O. K. Farha, *Adv. Mater.*, 2024, **36**, 2300951.
6 X. Yuan, J. Xiong, X. Wu, N. Ta, S. Liu, Z. Li and W.-Y. Lou, *Chem. Eng. J.*, 2024, **480**, 148246.
7 F. Xu, Q. Lu, P.-J. J. Huang and J. Liu, *Chem. Commun.*, 2019, **55**, 13215–13218.
8 M. H. Kuchma, C. B. Komanski, J. Colon, A. Teblum, A. E. Masunov, B. Alvarado, S. Babu, S. Seal, J. Summy and C. H. Baker, *Nanomedicine*, 2010, **6**, 738–744.
9 R. M. Bullock and A. Dey, *Chem. Rev.*, 2022, **122**, 11897–11899.
10 M. Zhao, H.-B. Wang, L.-N. Ji and Z.-W. Mao, *Chem. Soc. Rev.*, 2013, **42**, 8360–8375.
11 V. L. Schramm, *Annu. Rev. Biochem.*, 2011, **80**, 703–732.
12 B. de Souza, G. L. Kreft, T. Bortolotto, H. Terenzi, A. J. Bortoluzzi, E. E. Castellano, R. A. Peralta, J. B. Domingos and A. Neves, *Inorg. Chem.*, 2013, **52**, 3594–3596.
13 J. E. Coleman, *Annu. Rev. Biophys. Biomol. Struct.*, 1992, **21**, 441–483.
14 E. E. Kim and H. W. Wyckoff, *J. Mol. Biol.*, 1991, **218**, 449–464.
15 O. Iranzo, A. Y. Kovalevsky, J. R. Morrow and J. P. Richard, *J. Am. Chem. Soc.*, 2003, **125**, 1988–1993.
16 P. Solís Muñana, G. Ragazzon, J. Dupont, C. Z. Ren, L. J. Prins and J. L. Chen, *Angew. Chem. Int. Ed.*, 2018, **57**, 16469–16474.
17 J. Czescik, S. Zamolo, T. Darbre, F. Mancin and P. Scrimin, *Molecules*, 2019, **24**, 2814.
18 S. D. Pike, E. R. White, M. S. P. Shaffer and C. K. Williams, *Nat. Commun.*, 2016, **7**, 13008.
19 A. Krężel and W. Maret, *Arch. Biochem. Biophys.*, 2016, **611**, 3–19.
20 W. Maret and Y. Li, *Chem. Rev.*, 2009, **109**, 4682–4707.
21 B. M. Budhlall, K. Landfester, E. D. Sudol, V. L. Dimonie, A. Klein and M. S. El-Aasser, *Macromolecules*, 2003, **36**, 9477–9484.
22 M. van de Weert, J. Hoechstetter, W. E. Hennink and D. J. A. Crommelin, *J. Controlled Release*, 2000, **68**, 351–359.
23 H. S. Mansur, C. M. Sadahira, A. N. Souza and A. A. P. Mansur, *Mater. Sci. Eng. C*, 2008, **28**, 539–548. View Article Online DOI: 10.1039/D6DT00435K
24 H. Wang, T. Yang, J. Wang, Z. Zhou, Z. Pei and S. Zhao, *Chem*, 2024, **10**, 48–85.
25 R. R. Buchholz, et al., *Dalton Trans.*, 2008, 6045–6054.
26 S. Bosch, P. Comba, L. R. Gahan and G. Schenk, *Inorg. Chem.*, 2014, **53**, 9036–9051.
27 L. L. Mendes, D. Englert, C. Fernandes, L. R. Gahan, G. Schenk and A. Horn, *Dalton Trans.*, 2016, **45**, 18510–18521.
28 J. Czescik, Y. Lyu, S. Neuberg, P. Scrimin and F. Mancin, *J. Am. Chem. Soc.*, 2020, **142**, 6837–6841.
29 N. B. Rego and A. J. Patel, *Annu. Rev. Condens. Matter Phys.*, 2022, **13**, 303–324.
30 P. F. Fitzpatrick, *Biochim. Biophys. Acta, Proteins Proteomics*, 2015, **1854**, 1746–1755.
31 W. D. Guerra, E. Odella, M. Secor, J. J. Goings, M. N. Urrutia, B. L. Wadsworth, M. Gervaldo, L. E. Sereno, T. A. Moore, G. F. Moore, S. Hammes-Schiffer and A. L. Moore, *J. Am. Chem. Soc.*, 2020, **142**, 21842–21851.
32 A. Blanes-Díaz, M. Shohel, N. T. Rice, I. Piedmonte, M. A. McDonald, K. Jorabchi, S. A. Kozimor, J. A. Bertke, M. Nyman and K. E. Knope, *Inorg. Chem.*, 2024, **63**, 9406–9417.
33 F. Aubriet, J.-J. Gaumet, W. A. de Jong, G. S. Groenewold, A. K. Gianotto, M. E. McIlwain, M. J. Van Stipdonk and C. M. Leavitt, *J. Phys. Chem. A*, 2009, **113**, 6239–6252.
34 W. Chen, Y. Kitamura, J.-M. Zhou, J. Sumaoka and M. Komiyama, *J. Am. Chem. Soc.*, 2004, **126**, 10285–10291.

View Article Online
DOI: 10.1039/D6DT00435K

Data availability

The data supporting this article have been included as part of the SI. The supporting information contains experimental details on polymer preparation and characterization, spectroscopic analyses, catalytic assays.